View metadata, citation and similar papers at core.ac.uk
brought to you by CORE
provided by University of Waterloo's Institutional Repository

Accurate determination of interface trap state parameters by admittance spectroscopy in the presence of a Schottky barrier contact: Application to ZnO-based solar cells

Andrew T. Marin, Kevin P. Musselman, and Judith L. MacManus-Driscoll

Citation: Journal of Applied Physics **113**, 144502 (2013); doi: 10.1063/1.4799633
View online: https://doi.org/10.1063/1.4799633
View Table of Contents: http://aip.scitation.org/toc/jap/113/14
Published by the American Institute of Physics

Articles you may be interested in

Determination of defect distributions from admittance measurements and application to Cu(In,Ga)Se_2 based heterojunctions
Journal of Applied Physics **80**, 4411 (1996); 10.1063/1.363401

Interpretation of admittance, capacitance-voltage, and current-voltage signatures in Cu(In, Ga)Se_2 thin film solar cells
Journal of Applied Physics **107**, 034509 (2010); 10.1063/1.3277043

Investigation of defects by admittance spectroscopy measurements in poly (3-hexylthiophene):(6,6)-phenyl C_{61}-butyric acid methyl ester organic solar cells degraded under air exposure
Journal of Applied Physics **110**, 094509 (2011); 10.1063/1.3658023

Admittance spectroscopy of impurity levels in Schottky barriers
Journal of Applied Physics **46**, 2204 (1975); 10.1063/1.321865

Bulk and metastable defects in $CuIn_{1-x}Ga_xSe_2$ thin films using drive-level capacitance profiling
Journal of Applied Physics **95**, 1000 (2004); 10.1063/1.1633982

Defect density and dielectric constant in perovskite solar cells
Applied Physics Letters **105**, 153502 (2014); 10.1063/1.4897329

This article may be downloaded for personal use only. Any other use requires prior permission of the author and AIP Publishing. The following article appeared in Marin, A. T., Musselman, K. P., & MacManus-Driscoll, J. L. (2013). Accurate determination of interface trap state parameters by admittance spectroscopy in the presence of a Schottky barrier contact: Application to ZnO-based solar cells. Journal of Applied Physics, 113(14), 144502 and may be found at https://doi.org/10.1063/1.4799633

PHYSICS TODAY
WHITEPAPERS
MANAGER'S GUIDE
Accelerate R&D with Multiphysics Simulation
READ NOW
PRESENTED BY

JOURNAL OF APPLIED PHYSICS **113**, 144502 (2013)

Accurate determination of interface trap state parameters by admittance spectroscopy in the presence of a Schottky barrier contact: Application to ZnO-based solar cells

Andrew T. Marin,[1] Kevin P. Musselman,[2] and Judith L. MacManus-Driscoll[1,a)]
[1]*Materials Science & Metallurgy, University of Cambridge, Cambridge CB2 3QZ, United Kingdom*
[2]*Cavendish Laboratory, University of Cambridge, Cambridge CB3 0HE, United Kingdom*

(Received 29 January 2013; accepted 21 March 2013; published online 9 April 2013)

This work shows that when a Schottky barrier is present in a photovoltaic device, such as in a device with an ITO/ZnO contact, equivalent circuit analysis must be performed with admittance spectroscopy to accurately determine the pn junction interface recombination parameters (i.e., capture cross section and density of trap states). Without equivalent circuit analysis, a Schottky barrier can produce an error of ∼4-orders of magnitude in the capture cross section and ∼50% error in the measured density of trap states. Using a solution processed ZnO/Cu_2O photovoltaic test system, we apply our analysis to clearly separate the contributions of interface states at the pn junction from the Schottky barrier at the ITO/ZnO contact so that the interface state recombination parameters can be accurately characterized. This work is widely applicable to the multitude of photovoltaic devices, which use ZnO adjacent to ITO. © *2013 American Institute of Physics.* [http://dx.doi.org/10.1063/1.4799633]

I. INTRODUCTION

Recombination at interface states is highly disabling to the performance of a photovoltaic device and is particularly prevalent in many new-age device designs.[1,2] In order to better understand the impact of interface recombination on a device's performance, it is critical to determine the interface trap state density, capture cross section, and interface Fermi level position. These parameters directly influence the recombination velocity and dark saturation current, which impacts the photovoltaic device behavior.[3]

Admittance spectroscopy is a highly valuable technique that can be used to obtain the recombination parameters for a trap state.[4–8] These parameters can be determined by correlating a trap state's peak in the admittance data (usually plotted as the conductance[9] or differential capacitance[7]) with temperature. Admittance spectroscopy has been used to examine the bulk and interface state densities of multiple photovoltaic devices,[4–6,10] such as those employing CIGS as an absorber layer.

In addition, a Schottky barrier contact is known to produce a peak in the admittance data that resembles a trap state.[8,11,12] Schottky barrier contacts commonly exist in photovoltaic devices at the interface between a transparent conductor (e.g., ITO) and an n-type window layer (e.g., ZnO and TiO_2).[1,13] These contacts are ubiquitously used in multiple types of solar cells including bulk-heterojunction (e.g., ITO/ZnO/P3HT:PCBM),[14] thin film (e.g., ITO/ZnO/CdS/CIGS),[15] and quantum dot (e.g., ITO/ZnO/PbS)[16] devices. In a device with interface states and a Schottky barrier, two peaks will be observed in the admittance data. While the admittance behavior of the Schottky barrier contact is known,[11,12] the error induced by the Schottky barrier on a true trap state's recombination parameters has not been assessed.

A need for low-cost photovoltaics has pushed research towards solution processing at low temperatures and atmospheric pressure, but these cells are often hindered by interface defect states. These devices also often employ an ITO/ZnO contact. It is thus essential to understand the impact of the ITO/ZnO Schottky barrier on the analysis of interface states so that the electrical behavior of the device can be properly characterized.

We employ equivalent circuit analysis to understand the impact of the Schottky barrier on a trap state's recombination parameters as determined by admittance spectroscopy. For equivalent circuit analysis, an electrical circuit is created to describe the physical parameters in a device. For example, a parallel RC circuit can be used to describe a Schottky barrier contact.[1] While equivalent circuit analysis is rudimentary to the development of all dielectric techniques (impedance, admittance, modulus, and dielectric spectroscopy),[17] it is rarely[18] employed with admittance spectroscopy. As we show in this investigation, equivalent circuit analysis is a critical supplement to admittance spectroscopy when a Schottky barrier is present in a device.

We show the benefit of the combination of techniques when analyzing the interface recombination parameters of a solution deposited ZnO/Cu_2O device with an ITO/ZnO Schottky barrier contact. Fully electrodeposited ZnO/Cu_2O has gained recent interest as a low-cost photovoltaic device but has so far failed to reach its theoretical efficiency.[1,19–23] Many researchers attribute poor device performance of ZnO/Cu_2O to acceptor states at the heterojunction interface where electrons from the ZnO can become trapped and eventually recombine with holes from the Cu_2O.[1,24–26] The interface states are believed to originate from the lattice mismatch of the two materials[27] and from ZnO dissolution in the basic

[a)]Author to whom correspondence should be addressed. Electronic mail: jld35@cam.ac.uk

 © 2013 American Institute of Physics

Cu_2O deposition solution.[1] In addition, electrodeposited ZnO has a high surface defect density due to $Zn(OH)_2$ formation which has been shown to degrade the performance of ZnO/bulk-heterojunction cells[14] and is expected to contribute to the interface trap state density in ZnO/Cu_2O as well. While researchers have discussed the origin of the interface trap states, the recombination parameters of this device have not been measured.

This investigation is broken into 4 parts. We first examine the theory of using admittance spectroscopy to measure interface recombination parameters (Sec. III A). We then analyze how a Schottky barrier can alter the apparent trap state's differential capacitance response (Sec. III B) and show the significant error in the recombination parameters if the Schottky barrier is not subtracted (Sec. III C). Finally, in Sec. IV we employ the combination of equivalent circuit analysis and admittance to accurately measure the density of trap states and capture cross section of a ZnO/Cu_2O device for the first time.

II. EXPERIMENTAL

Glass/ITO substrates from Präzisions Glas & Optik were cleaned in an ultrasonic bath in water, acetone, and isopropanol for 15 min each. ZnO films were grown on the ITO via potentiostatic deposition at −0.85 V vs a Ag/AgCl (saturated KCl) reference electrode,[28] in a 0.08 M $Zn(NO_3)_2$ solution with 15% volume ethanol at a temperature of $70 \pm 1\,°C$. Films were grown to an approximate thickness of 500 nm. Cu_2O was deposited galvanostatically onto the ZnO films at −1.0 mA cm^{-2} from an aqueous solution of 0.04 M Cu_2SO_4/3 M lactic acid at 40 °C.[20] The pH was adjusted to 12.6 by adding 4 M NaOH. Films were grown to a thickness of 3 μm. Gold contacts were evaporated on the Cu_2O using a BOC Edwards Auto 306 resistance evaporator. The device area was 0.15 cm^2.

The trap state density was examined by admittance spectroscopy. Samples were analyzed from 40 Hz to 1 MHz with a 20 mV AC voltage using an Agilent 4294 A impedance analyzer. The temperature was controlled using a hot plate, and samples were kept in the dark for 48 h prior to testing the device in order to empty states filled from photogenerated charges. The LEVMW complex nonlinear least squares fitting software was used to fit the admittance data for equivalent circuit analysis.[17]

The carrier density of electrodeposited Cu_2O and ZnO has to have previously been measured to be $<10^{14}$ cm^{-3} and $>10^{17}$ cm^{-3}, respectively.[19,21] This 3-4 order of magnitude difference creates an n^+-p structure where the depletion width of the ZnO region is negligible (~1 nm) in comparison to the depletion width of Cu_2O (1.5–3 μm), considering the built-in potential (0.4–0.7 eV) and the dielectric constants ($7\varepsilon_0$ Cu_2O, $8\varepsilon_0$ ZnO) of the two materials.[21,24]

III. THEORY AND MODELING

A. Measuring interface states by admittance spectroscopy

During an admittance spectroscopy measurement, an applied AC voltage oscillates the Fermi level of the device under test at a given frequency. From the measured admittance, the capacitance which relates to the charge density of the semiconductor region being analyzed is calculated. For an abrupt pn junction with a p-region carrier density much less than the n-region carrier density (n^+-p junction), charges in the valence band will only contribute to the measured capacitance response if they exist at a position in the junction where the difference between the Fermi level and valence band energy is small enough for the charges to follow the oscillation, depicted by the shaded region in Figure 1.

Equation (1) describes the relationship between the measurement frequency (ω) and the energy difference (E_ω) at a position x_ω in the junction[7]

$$\omega = 2N_V v_{th}\sigma_c e^{(-E_\omega/kT)} = \xi T^2 e^{(-E_\omega/kT)}. \tag{1}$$

When sweeping across a range of frequencies, an increase in capacitance will occur at the location corresponding to the position that a trap state crosses the Fermi level (x_0 in Figure 1).[4,7,29] A differential capacitance plot ($\omega \cdot dC/d\omega$ versus ω) will result in a peak at the emission frequency ($\omega = \omega_0$) of the trap state. If the measurement is performed for a range of temperatures (T), an Arrhenius plot of Eq. (1) can reveal the energy position ($E_\omega = E_0$) and emission prefactor ($\xi = \xi_0$) of a trap state.[7] The emission prefactor represents the temperature independent parts of the effective density of states for the valence band (N_V), the thermal velocity (υ_{th}), and the capture cross section (σ_c).

In order to differentiate bulk from interfacial trap states, admittance measurements should be performed at different biases. The energy of the trap state (E_0) will be equal to the difference between the Fermi level and the valence band at the location x_0. Bulk states are generally energetically discrete. Thus, their trap state energy should be bias

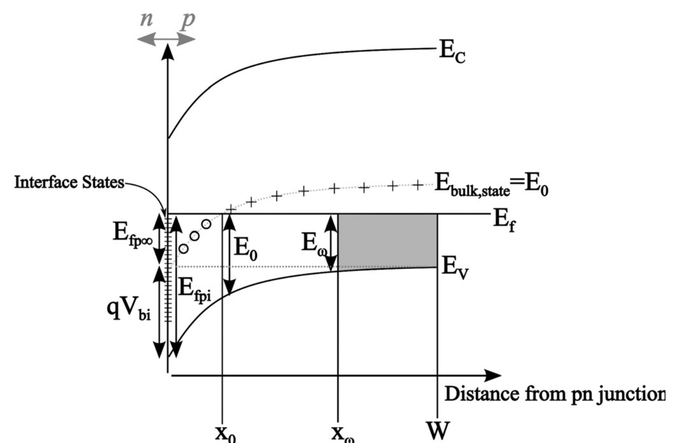

FIG. 1. Schematic of a band diagram of the p-side of an abrupt n^+-p junction (such as in ZnO/Cu_2O). The shaded region represents the region contributing to the capacitance when measuring at a frequency (ω) during admittance spectroscopy. The frequency translates into an energy (E_ω) which represents the difference between the Fermi level and the valence band at a location (x_ω). Here, a bulk trap state is shown to exist at an energy (E_0) above the valence band and cross the Fermi level at a position (x_0). A trap state will only contribute to the capacitance response if the frequency is low enough to encompass a region stretching to x_0 from the depletion width edge (W). Additionally, it can be seen that the energy at the interface (E_{fpi}) is equal to the built-in potential energy (qV_{bi}) plus the bulk Fermi level position ($E_{fp\infty}$).

independent.[29,30] Conversely, interface states will correspond to the interface Fermi level position ($E_{fpi} = E_0 = E_\omega$) which is defined by

$$E_{fpi} = E_{fp\infty} + qV_{bi}. \tag{2}$$

In this equation, $E_{fp\infty}$ is the bulk Fermi level position and V_{bi} is the built-in potential. Since V_{bi} varies with bias, E_{fpi} will also be bias dependent,[7,29,30] as long as the Fermi level is not pinned at the interface.[4]

Equation (3) can be used to determine the density of interface trap states from the device area (A) and trap state capacitance (C_t), which is equivalent to $-2\omega dC/d\omega$ upon differentiation of the equivalent circuit model for a pn junction containing interface states (discussed more in Sec. III B).[9] Subsequently, Eq. (1) can be used to transform the frequency into an energy axis

$$N_t(E_\omega) = \frac{C_t}{q^2 A} = \frac{-2\omega}{q^2 A}\frac{dC}{d\omega}. \tag{3}$$

Recombination at interface states can dictate the behavior of the pn junction diode.[2] For an n^+-p junction, electrons from the n-material will become trapped at interface states. Recombination will therefore be limited by holes from the p-material finding a filled trap state at the interface. The resulting saturation current density summarizing this mechanism is given by[3]

$$J^0_{pn} = qp_{if}S, \tag{4}$$

where S is the recombination velocity defined by

$$S = \sigma_c v_{th} N_t, \tag{5}$$

and p_i is the density of holes at the interface defined by

$$p_i = N_V e^{-qE_{fpi}/kT}. \tag{6}$$

The saturation current density (Eq. (4)) can then be calculated from the admittance results using the capture cross section and thermal velocity (Eq. (1)), the interface Fermi level energy (Eq. (2)), and the interface state charge density which can be obtained by integrating the density of states (Eq. (3)) in energy.

B. Influence of a Schottky barrier contact on differential capacitance

In Sec. III A, we described how a differential capacitance plot ($\omega dC/d\omega$ vs. ω) can be used to obtain the interface trap state recombination parameters. One disadvantage of this plot is the blind assessment of the "trap" state peaks. Other researchers[11,12,31] have shown that a Schottky barrier contact can also produce a peak alongside an apparent trap state peak in a differential capacitance plot. What has not been discussed is the error induced by the Schottky barrier contact on the apparent trap state's peak magnitude and frequency, which are used to calculate the recombination parameters.

To assess this error, we consider the equivalent circuit model in Figure 2. Capacitor (C_j) is the junction capacitance

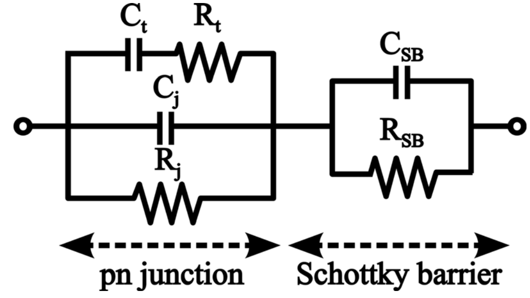

FIG. 2. Equivalent circuit model of a pn junction with a trap state in series with a Schottky barrier contact. C_j is the junction capacitance and R_j is the parallel resistance of the pn junction depletion region. C_t is the trap state capacitance and R_t is the resistance to recombination. C_{SB} is the capacitance and R_{SB} is the parallel resistance of the Schottky barrier depletion region.

representing free carriers in the depletion region and R_j is the parallel shunt resistance. A third branch is shown which contains the trap state capacitance (i.e., $C_t \propto$ density of trap states—Eq. (3)) and the resistance to recombination (R_t). In the second section, C_{SB} is the capacitance and R_{SB} is the parallel resistance across the Schottky barrier depletion region. The total capacitance as a function of frequency for the model in Figure 2 is derived in Appendix A.

Figure 3(a) shows a modeled differential capacitance plot for a device with a trap state in the absence of a Schottky barrier contact and two cases for devices with a trap state in the presence of a Schottky barrier. The differential capacitance in the absence of the Schottky barrier has one peak at frequency $\omega_0 \sim 2.5 \times 10^4$ rad s^{-1} and a peak magnitude of $P = 4.5 \times 10^{-9}$ F cm^{-2} (i.e., $C_t/2$—Eq. (3)). When the Schottky barrier is added to the model, many different scenarios exist depending on the relative magnitude of C_j vs. C_t vs. C_{SB} and τ_j vs τ_t vs τ_{SB} where $\tau_i = R_i C_i$.

We consider two plausible cases: Case 1 [$C_t > C_{SB} > C_j$, $\tau_t > \tau_{SB} > \tau_j$] and Case 2 [$C_{SB} > C_t > C_j$, $\tau_{SB} > \tau_t > \tau_j$]. Case 1 represents a device with interface states and a Schottky barrier in the n^+-material which has a doping density that gives a moderately large (100-500 nm) Schottky barrier depletion width but is less than the depletion width of the pn junction. Case 2 represents a device with an equal number of interface trap states as Case 1 but has a higher carrier concentration, higher dielectric constant, or lower barrier height in the Schottky barrier depletion region than Case 1 such that C_{SB} is larger than C_t.

For Case 1, the differential capacitance plot has two peaks as shown in Figure 3(a). Both peaks are composed of contributions from the trap state and Schottky barrier. The apparent trap state peak (ω_0',P′) is much lower in magnitude and frequency than the true trap state peak (ω_0,P). The reduction of the trap state magnitude results from the change in the maximum capacitance and the creation of an intermediate capacitance level (C_{mid}) when a Schottky barrier is present in the device (Figure 3(b)). In the absence of a Schottky barrier contact, the capacitance is equal to the junction capacitance (C_j) for high frequencies and increases to the junction plus the trap state capacitance ($C_j + C_t$) at low frequencies. In the presence of a Schottky barrier contact, it can be derived (see Appendix A) that the maximum capacitance is equivalent to

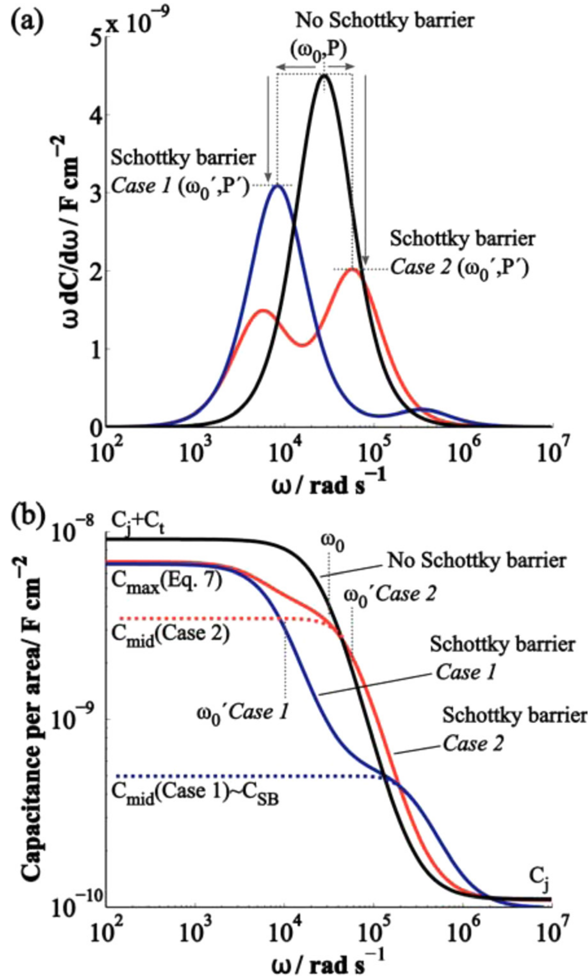

FIG. 3. (a) Modeled differential capacitance for a device with a trap state in the absence and presence of a Schottky barrier contact. In the absence of a Schottky barrier, the trap state peak magnitude and frequency exist at the location (ω_0,P). In the presence of a Schottky barrier, the apparent trap state peak moves to a location (ω_0',P′). (b) Capacitance versus frequency for the same devices modeled in (a).

$$C_{\max} = \frac{C_{SB}R_{SB}{}^2 + (C_j + C_t)R_j{}^2}{(R_{SB} + R_j)^2}. \quad (7)$$

The differential capacitance corresponding to the apparent trap state in Case 1 will thus represent the change from $C_{mid} \sim C_{SB}$ to C_{max} (i.e., $\omega \cdot dC/d\omega \sim \omega \cdot \Delta(C_{max} - C_{SB})/\Delta\omega$). Since $C_{SB} > C_j$ and $C_{max} < C_j + C_t$, the peak in the differential capacitance plot is lowered when a Schottky barrier is present in the device. The presence of R_{SB} also pushes the peak to a lower frequency ($\omega_0' < \omega_0$). Larger values of R_{SB} push ω_0' further away from ω_0. In the supplementary material,[32] we present the percent error of the trap state peak magnitude and frequency as a function of each of the circuit model parameters.

Case 2 ($C_{SB} > C_t > C_j$, $\tau_{SB} > \tau_t > \tau_j$) exemplifies that the apparent trap state peak can also exist at a frequency greater than ω_0 for a different set of capacitances and time constants. For this case, the differential capacitance will correspond to the change from the minimum capacitance (~Cj) to C_{mid}. Since $C_{mid} < C_j + C_t$, P′ < P similar to Case 1. Unlike Case 1, C_{SB} is more influential than R_{SB} in Case 2 on the apparent trap state peak frequency (ω_0'). Smaller values of C_{SB} push ω_0' further from ω_0. As we show in Secs. III C and IV, it is necessary to perform equivalent circuit analysis to identify the apparent trap state peak and separate the contributions of the different circuit elements.

C. Modeled influence of a Schottky barrier contact on the density of states, capture cross section, and trap state energy

In this section, we model the impact of the Schottky barrier on the measured trap state recombination parameters by considering how the temperature dependence of the Schottky barrier circuit elements alters the expected temperature-frequency relationship (Eq. (1)) of the apparent trap state peak. We consider temperature dependent resistance [$R_t(T)$, $R_{SB}(T)$, and $R_j(T)$] with either (1) temperature *independent* capacitance [C_t, C_{SB}, and C_j] or (2) temperature *dependent* capacitance [$C_t(T)$, $C_{SB}(T)$, and $C_j(T)$].

The temperature dependence of R_t can be defined by Eqs. (1), (8), and (9), which relates $R_t(T)$ to $\omega_0(T)$ and $C_t(T)$

$$\omega_0 = \frac{1}{\tau_t} = \frac{1}{R_t C_t}, \quad (8)$$

$$R_t(T) = (C_t(T)\omega_0)^{-1} = (C_t(T)\xi_0 T^2 e^{-E_0/kT})^{-1}. \quad (9)$$

The occupancy of interface states is expected to be a function of the free carrier density at the interface, particularly that of the more highly doped side of the pn junction. For an n^+-p junction, we consider $C_t(T) \propto n_i(T)$ defined by[33]

$$C_t(T) \propto n_i(T) = N_C e^{-E_{fni}/kT} = A_t T^{1.5} e^{-E_{fni}/kT}, \quad (10)$$

where A_t is a temperature independent constant, E_{fni} is the interface Fermi level position in the n-material, and N_C is effective density of states in the conduction band which has a temperature dependence[33] of $T^{1.5}$. Likewise, the temperature dependence of $C_{SB}(T)$ is related to the free carrier density of the bulk n-material, $N_D(T)$, by

$$C_{SB}(T) = \frac{\varepsilon_{SB}A}{W_{SB}} = \sqrt{\frac{q\varepsilon_{SB}N_D(T)A^2}{2\Phi_{SB}}} = A_{SB,C}\sqrt{T^{1.5}e^{-E_{fn\infty}/kT}}. \quad (11)$$

The temperature independent pieces of the dielectric constant (ε_{SB}), depletion width (W_{SB}), and barrier height (Φ_{SB}) are summarized by $A_{SB,C}$. $E_{fn\infty}$ is the bulk Fermi level position in the n-material and A is the area of the sample.

We assume that conduction over the Schottky barrier occurs via thermionic emission.[33] Thus $R_{SB}(T)$ will behave in accordance with Eq. (12),[12] with a constant $A_{SB,R}$

$$R_{SB}(T) = A_{SB,R}T^{-1}e^{\Phi_{SB}/kT}. \quad (12)$$

The temperature dependent junction capacitance (Eq. (13)) will behave in the same manner as C_{SB} (Eq. (11)), but will be dependent on the p-material concentration, $N_A(T)$, with constant $A_{SB,j}$

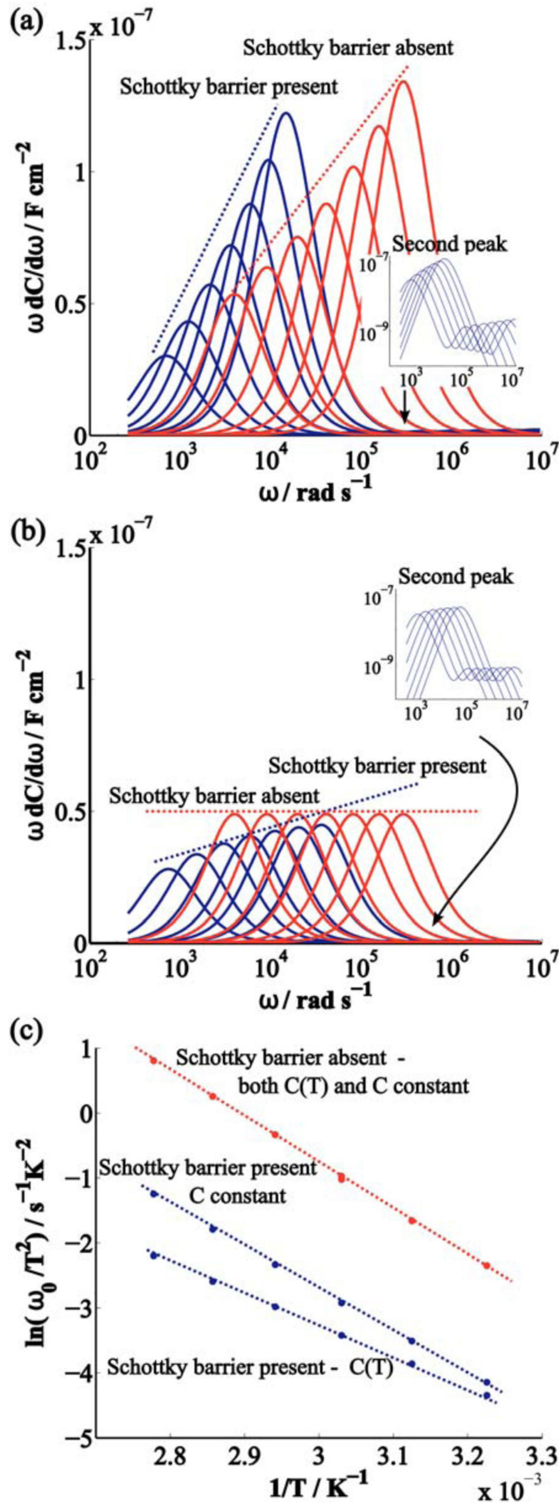

FIG. 4. Modeled differential capacitance plots of the equivalent circuit in Figure 2 considering (a) temperature dependent C_t, C_{SB}, and C_j and (b) temperature independent $C_t(T)$, $C_{SB}(T)$, and $C_j(T)$. For both (a) and (b), the plots show the differential capacitance at different temperatures in the presence (blue) and absence (red) of the Schottky barrier. Arrhenius plots based on Eq. (1) of the four scenarios are given in (c). For the temperature independent scenarios, $C_t = 9.8 \times 10^{-8}\,\mathrm{F\,cm^{-2}}$, $C_{SB} = 4.3 \times 10^{-9}\,\mathrm{F\,cm^{-2}}$, $C_j = 2.6 \times 10^{-6}\,\mathrm{F\,cm^{-2}}$. Model parameters were used to give roughly equivalent capacitance and resistance values between the temperature independent and dependent scenarios at 300 K. Model parameters are $A_{t,C} = 9.9 \times 10^{-10}\,\mathrm{F\,cm^{-2}\,K^{-2}}$, $E_{fpi} = 0.61\,\mathrm{eV}$, $\sigma_C = 6.3 \times 10^{-13}\,\mathrm{cm^2}$, $A_{SB,C} = 4.3 \times 10^{-9}\,\mathrm{F\,cm^{-2}\,K^{4/3}}$, $E_{fn\infty} = 0.1\,\mathrm{eV}$, $\Phi_{SB} = 0.6\,\mathrm{eV}$, $A_{SB,R} = 3.4 \times 10^{-4}\,\Omega\,\mathrm{cm^2\,K}$, $C_{j,C} = 1.4 \times 10^{-8}\,\mathrm{F\,cm^{-2}\,K^{4/3}}$, $E_{fp\infty} = 0.37\,\mathrm{eV}$, $A_{j,R} = 1 \times 10^{-9}\,\Omega\,\mathrm{cm^2}$, $T_{j,R} = 30\,\mathrm{K}$.

$$C_j(T) = \frac{\varepsilon_j A}{W_j} = \sqrt{\frac{q\varepsilon_j N_A(T) A^2}{2\Phi_j}} = A_{SB,j}\sqrt{T^{1.5} e^{-E_{fp\infty}/kT}}. \quad (13)$$

Lastly, $R_j(T)$ is defined by the following equation with constants A_j and T_j as has been observed elsewhere for polycrystalline semiconductors[34]

$$R_j(T) = A_j e^{-T/T_j}. \quad (14)$$

Figure 4 shows the differential capacitance calculated at different temperatures in the presence and absence of a Schottky barrier for the temperature dependent capacitance scenario (Figure 4(a)) and temperature independent capacitance scenario (Figure 4(b)). As for Figure 3, the presence of the Schottky barrier is seen to change the magnitude and frequency position of the apparent trap state peak at each temperature. The capture cross section (σ_C) and trap state energy (E_0) were calculated from an Arrhenius plot of Eq. (1) for all four models (Figure 4(c)). The maximum density of trap states was also estimated from the peak value at 300 K.

As shown in Table I, the model recombination parameters ($E_0 = E_{fpi} = 0.61\,\mathrm{eV}$, $\sigma_C = 6.3 \times 10^{-13}\,\mathrm{cm^2}$, and $N_t(300\,\mathrm{K}) = 6.1 \times 10^{12}\,\mathrm{cm^{-2}\,eV^{-1}}$) were reproduced within 1% by the Arrhenius plot for both temperature independent and temperature dependent capacitance scenarios in the absence of the Schottky barrier. However, in the presence of the Schottky barrier, all three recombination parameters were vastly different from the input values. A reduction in the observed density of trap states resulted from the reduced peak magnitude ($P' < P$). The percent error was found to be similar for both scenarios (~50%).

The interface energy and capture cross section obtained from the apparent trap state peaks were also largely different from the input parameters. For temperature independent capacitances, the error in the trap state energy was ~10% and capture cross section was ~100%. For temperature dependent capacitances, the error was much worse, reaching ~32% in trap state energy (0.41 eV vs 0.61 eV input) and ~4-orders of magnitude difference ($5.6 \times 10^{-17}\,\mathrm{cm^2}$ vs $6.3 \times 10^{-13}\,\mathrm{cm^2}$ input) in the capture cross section.

The error in both scenarios is largely due to the temperature dependence of R_{SB}. Since, the apparent trap state peak will be a mixture of contributions from the trap state and Schottky barrier, and since R_{SB} (Eq. (12)) obeys a different temperature relationship than R_t (Eq. (9)), the temperature dependence of the apparent peak frequency (ω_0') and hence the recombination parameters obtained by fitting to an Arrhenius plot (Eq. (1)) will be different than in the absence of a Schottky barrier. When $C_{SB}(T)$ and $C_t(T)$ also have different temperature relationships, an Arrhenius plot of the apparent trap state peak frequency deviates even further from the appropriate correlation. Due to the expected temperature dependence of interface states (Eq. (10)), it is clear that the Schottky barrier contact contribution must be subtracted. Additionally, since the product of the recombination parameters can be used to estimate the dark saturation current (Eq. (4)), the error in measuring the recombination parameters can lead to a very inaccurate assessment of the device performance.

TABLE I. Comparison of the trap state energy (E_0), capture cross section (σ_C), and density of states (N_t) for different models considering temperature independent and dependent capacitance in the presence and absence of a Schottky barrier contact.

Model	E_0 (eV)	σ_C (cm^2)	N_t at 300 K (cm^{-2} eV^{-1})
Temperature independent capacitance			
Input	*0.61*	*6.3×10^{-13}*	*6.1×10^{12}*
Schottky barrier absent	0.61	6.3×10^{-13}	6.1×10^{12}
Schottky barrier present	0.55	1.1×10^{-14}	3.5×10^{12}
Temperature dependent capacitance			
Input	*0.61*	*6.3×10^{-13}*	*6.6×10^{12}*
Schottky barrier absent	0.61	6.3×10^{-13}	6.6×10^{12}
Schottky barrier present	0.41	5.6×10^{-17}	3.9×10^{12}

IV. TEST CASE: USING EQUIVALENT CIRCUIT MODELING WITH ADMITTANCE SPECTROSCOPY TO MEASURE INTERFACE STATE PARAMETERS IN A SOLUTION PROCESSED ZnO/Cu$_2$O DEVICE IN THE PRESENCE OF AN ITO/ZnO SCHOTTKY BARRIER

In this section, we use equivalent circuit modeling to eliminate the effects of an ITO/ZnO Schottky barrier for analyzing interface state properties in a ZnO/Cu$_2$O device measured by admittance spectroscopy. The density and capture cross section of any trap state are important parameters that will allow more accurate modeling of the device response in the future using simulation programs such as SCAPS.[35]

Three equivalent circuit models (Figures 5(a)–5(c)) were fit to the raw admittance data using the LEVMW nonlinear least squares regression fitting software.[17] As noted in Sec. II, the ZnO carrier density is multiple orders of magnitude greater than the Cu$_2$O carrier density. Thus, the n-region capacitance was neglected from the models for equivalent circuit analysis. Figure 5(a) shows a simple circuit model similar to Figure 2 with additional series resistance (R_S) due to conduction through the neutral semiconductor regions and inductance (L) of the wires between the instrument and the device. The simple model, however, was found to be a poor representation of the experimental data with up to a 25% error (Figure 5(d)) for some frequencies.

While the ultimate goal for photovoltaics is low-temperature, scalable growth such as by solution deposition, semiconductors produced by solution deposited techniques are known to be inhomogeneous due to the polycrystalline growth[21,36] and large concentration of hydroxyl groups[28,36] that can become trapped in the films. The constant phase element (CPE) is a versatile distributed element that has previously been used by our group to describe the inhomogenities in the ZnO film of the ITO/ZnO Schottky barrier.[1] The impedance of the CPE is given by Eq. (15),[17]

$$Z_{CPE} = \frac{1}{Q(j\omega)^n} = \left(Q\omega^n\left[\cos\left(\frac{\pi n}{2}\right) + j\sin\left(\frac{\pi n}{2}\right)\right]\right)^{-1}. \quad (15)$$

In this equation, n is an ideality factor with values between 0 and 1. For n = 1, the CPE represents a pure capacitance with Q = C. For n = 0, the CPE is a pure resistor with Q = 1/R.

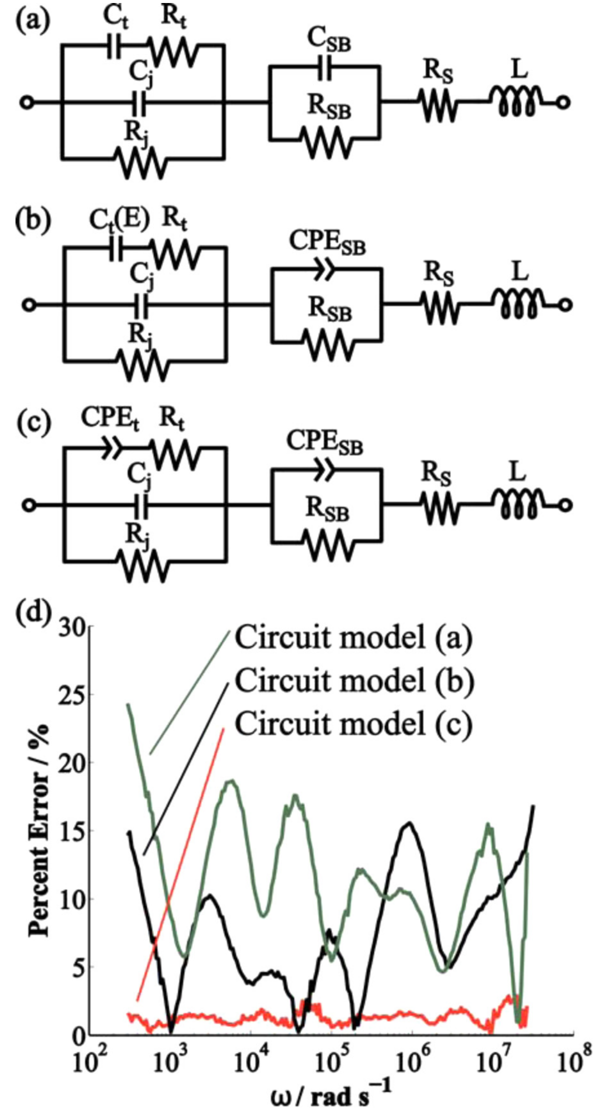

FIG. 5. (a)-(c) Equivalent circuit models and (d) percent error (100% * |Model − Data|/Data) of the magnitude of admittance versus frequency at 300 K. Circuit model (a) uses a pure capacitor for C_t and C_{SB}. Circuit model (b) uses a CPE to replace C_{SB} and a Gaussian distribution of states for C_t. Circuit model (c) uses a CPE for C_t and C_{SB}.

Lateral inhomogeneity at the pn junction interface is also expected to exist in solution deposited samples.[1] Other researchers[2,37,38] have discussed the influence of lateral inhomogeneity on the device electric behavior and have suggested using a Gaussian function[2,37] to represent a broad distribution of band levels that can exist at the interface. We find that the CPE can also describe the interface energy variability. Good fits (<3% error for all frequencies) were obtained for the electrodeposited ZnO/Cu$_2$O system when using the CPE (Figure 5(d)).

Admittance data modeled using the equivalent circuit in Figure 5(c) were found to accurately reproduce the raw data for all temperatures (Figure 6). The resulting fit parameters and error are given in Appendix B. It is noted that a junction capacitance of $\sim 4 \times 10^{-9}$ F cm^{-2} was obtained which gives a depletion width of 1.6 μm and matches well with the expected depletion width (1.5-3 μm) based on the carrier densities of the ZnO and Cu$_2$O layers (Sec. II). The Schottky

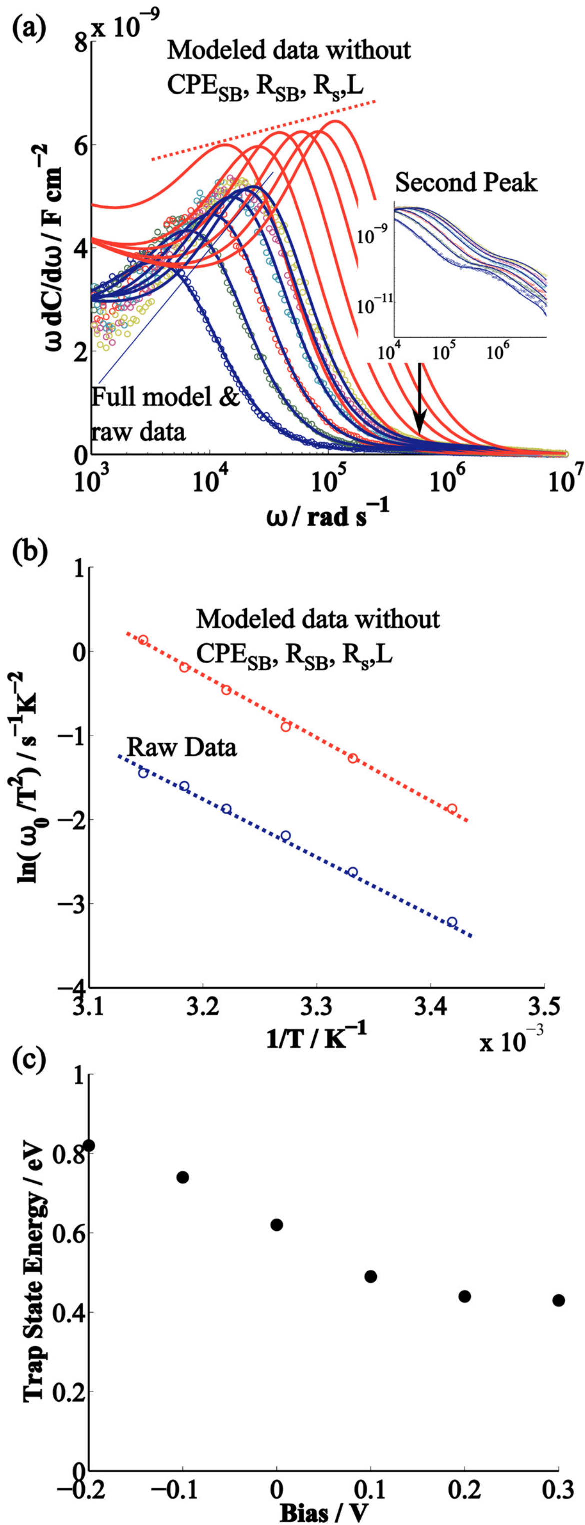

FIG. 6. (a) Admittance spectroscopy data of a ZnO/Cu_2O device with an ITO/ZnO Schottky barrier measured from 290-320 K (open circles). The full modeled data (blue lines) and modeled data without CPE_{SB}, R_{SB}, R_S, and L (red lines) are also presented. (b) Arrhenius plot of the trap state peak of the raw data (blue) and modeled data with the Schottky barrier, series resistance, or inductance contributions (red). (c) Correlation of the interface trap state energy with bias.

barrier, series resistance, and inductance were then subtracted so that only the pn junction and trap state contributions remained. The differential capacitance of the pn junction and trap state components (calculated from Eqs. (A1)-(A4)) at each temperature was calculated and re-plotted alongside the original data in Figure 6(a).

From an Arrhenius plot of Eq. (1) (Figure 6(b)), the energy and capture cross section were calculated from the trap state peak with and without equivalent circuit modeling. In addition, Figure 6(c) shows that the trap state energy is bias dependent, thus confirming that this trap state arises from a continuous distribution of trap states located at the pn junction interface as explained earlier in this work. The density of interface states was also estimated using Eq. (3) from the peak magnitude of the differential capacitance plots with and without equivalent circuit analysis. These results are presented in Table II.

Table II shows that the apparent density of interfacial trap states measured in the presence of the ITO/ZnO contact is ~30% lower than the value measured after equivalent circuit modeling. Likewise, the interface Fermi level position and capture cross section are also lower than the true value by ~10% (0.55 eV raw vs 0.62 eV model) and ~40-times (1.2×10^{-13} cm^2 raw vs 4.5×10^{-12} cm^2 model), respectively. These results are consistent with the theory presented in Secs. III A–III C. The temperature dependence of R_{SB} and C_{SB} changes the apparent trap state peak's expected temperature-frequency relationship (Eq. (1)) and produces an error in the measured recombination parameters.

Using Eq. (5), the interface recombination velocity (S) was calculated to be $\sim 7 \times 10^5$ cm s^{-1}. This recombination velocity is relatively high compared to other photovoltaic devices. Typically, vacuum-fabricated devices (such as in c-Si or GaAs-based devices) have recombination velocities below 10^5 cm s^{-1} with some reaching values on the order of 10^0 cm s^{-1} when passivation techniques are employed.[39,40]

Recombination velocity is proportional to the product of density of trap states and the capture cross section (Eq. (5)). Generally, the density of trap states and capture cross section have values between 10^{10}–10^{13} cm^{-2} eV^{-1} (density of states) and 10^{-20}–10^{-14} cm^2 (capture cross section).[41,42] As shown in Table II, the capture cross section is very large ($>1 \times 10^{-13}$ cm^2) for ZnO/Cu_2O and is the dominant contributor to the recombination velocity.

While it is unknown at this time what causes the large capture cross section, we speculate that this could arise from (1) clustering of trap states or (2) a low electric field at the pn junction interface. The capture cross section describes the area of influence of a trap state. If a free carrier passes through this area, the carrier can be coulombically attracted towards the charged trap and recombine. Clustered traps can act collectively, expressing a larger area of influence than an independent trap site. Due to the high defect concentrations present in ZnO[43] and Cu_2O,[44,45] it is reasonable to expect defects to migrate and cluster at the interface.

Capture cross section also describes the propensity of a free carrier's path to be influenced. A free carrier's path is less likely to be diverted when moving with a high velocity in the presence of an electric field. Due to the low free carrier density in Cu_2O ($\sim 1 \times 10^{14}$ cm^{-3}),[21,46] a low electric field ($\sim 10^3$ V cm^{-1}) is expected at the interface.

Lastly, it is noted that other trap states may exist. Due to the compensated nature of Cu_2O, ionized deep donor states

TABLE II. Summarized admittance spectroscopy results averaged (±1 standard deviation) for 3 ZnO/Cu_2O devices. Raw data include an ITO/ZnO Schottky barrier. Modeled data subtract the Schottky barrier contact as well as the additional series resistance and inductance.

	E_{fpi} (eV)	σ_C (cm^2)	Max N_t at 300 K (cm^{-2} eV^{-1})
Raw data	0.55 ± 0.03	$1.2 \times 10^{-13} \pm 1.0 \times 10^{-13}$	$1.8 \times 10^{11} \pm 4.5 \times 10^{10}$
Modeled data (R_{SB}, CPE_{SB}, R_S, L subtracted)	0.62 ± 0.02	$4.5 \times 10^{-12} \pm 3.2 \times 10^{-12}$	$2.6 \times 10^{11} \pm 7.4 \times 10^{10}$

can accept electrons and act as recombination centers.[44,45] However, it is apparent from the voltage dependence of the trap state energy (Figure 6(c)) that interface states are the dominant trap location in a fully electrodeposited ZnO/Cu_2O device.

V. CONCLUSIONS

Equivalent circuit analysis was shown to be an imperative supplement to admittance spectroscopy when analyzing recombination parameters of interface states in a pn junction solar cell containing a Schottky barrier contact. Both interface states and a Schottky barrier contact produced a response in the admittance data. Without equivalent circuit modeling, the temperature dependence of the Schottky barrier resistance and capacitance forced the apparent trap state response to deviate from its true frequency-temperature relationship. Modeling showed that this deviation could produce ∼4-orders of magnitude error in the measured capture cross section. By applying equivalent circuit modeling to a fully electrodeposited ZnO/Cu_2O device containing an ITO/ZnO Schottky barrier, we accurately determined the interface trap state recombination parameters and recombination velocity ($\sim 7 \times 10^5$ cm s^{-1}). The high recombination velocity, as expected for a solution deposited device, was mainly attributed to very large capture cross section ($\sim 5 \times 10^{-12}$ cm^2).

ACKNOWLEDGMENTS

The authors would like to acknowledge the International Copper Association, the ERC for the Advanced Investigator Grant, Novox, ERC-2009-adG 247276, the Gates Cambridge Trust, and Girton College (Cambridge) for funding this work.

APPENDIX A: SOLVING FOR THE MAXIMUM CAPACITANCE

Admittance spectroscopy relies on Eqs. (A1) and (A2) which define the admittance for a pn junction with a trap state

$$Y_{pn} = \frac{1}{Z_{pn}} = \frac{1}{R_t + (j\omega C_t)^{-1}} + \frac{1}{R_j} + j\omega C_j, \quad \text{(A1)}$$

$$Y_{pn} = G_{pn} + jB_{pn} = \frac{1}{R_j} + \frac{\omega^2 \tau_t C_t}{\omega^2 \tau_t^2 + 1} + j\left[\omega C_j + \frac{\omega C_t}{\omega^2 \tau_t^2 + 1}\right], \quad \text{(A2)}$$

where $\tau_t = R_t C_t$. The junction capacitance will be the susceptance (B) divided by the frequency, given by

$$C_{pn} = B_{pn}/\omega = C_j + \frac{C_t}{\omega^2 \tau_t^2 + 1}. \quad \text{(A3)}$$

Taking the derivative of this equation and multiplying by ω results in Eq. (A4) which gives the differential capacitance of a junction with a trap state. It can be shown that at $\omega_0 = 1/\tau_t$ (ω_0 defined by Eq. (1)) the peak of the differential capacitance will be equal to $C_t/2$ (Eq. (3))

$$\omega \frac{dC_{pn}}{d\omega} = \omega \frac{2C_t \omega \tau_t^2}{(\omega^2 \tau_t^2 + 1)^2}. \quad \text{(A4)}$$

The total capacitance changes if a Schottky barrier is present in the device according to the following equations:

$$Z_{Total} = Z_{SB} + Z_{pn}, \quad \text{(A5)}$$

$$Y_{SB} = \frac{1}{Z_{SB}} = \frac{1}{R_{SB}} + j\omega C_{SB}, \quad \text{(A6)}$$

$$Z_{SB} = \frac{R_{SB}}{1 + \omega^2 \tau_{SB}^2} - j\frac{\omega \tau_{SB} R_{SB}}{1 + \omega^2 \tau_{SB}^2}, \quad \text{(A7)}$$

$$Z_{total} = \frac{R_{SB}}{1 + \omega^2 \tau_{SB}^2} - j\frac{\omega \tau_{SB} R_{SB}}{1 + \omega^2 \tau_{SB}^2} + \frac{G_{pn}}{G_{pn}^2 + B_{pn}^2} - j\frac{B_{pn}}{G_{pn}^2 + B_{pn}^2}, \quad \text{(A8)}$$

$$Y_{total} = \frac{1}{Z_{total}} = G_{total} + jB_{total}, \quad \text{(A9)}$$

and

$$C_{total} = B_{total}/\omega = \frac{\frac{\tau_{SB} R_{SB}}{1 + \omega^2 \tau_{SB}^2} + \frac{C_{pn}}{G_{pn}^2 + B_{pn}^2}}{\left(\frac{R_{SB}}{1 + \omega^2 \tau_{SB}^2} + \frac{G_{pn}}{G_{pn}^2 + B_{pn}^2}\right)^2 + \left(\frac{\omega \tau_{SB} R_{SB}}{1 + \omega^2 \tau_{SB}^2} + \frac{B_{pn}}{G_{pn}^2 + B_{pn}^2}\right)^2}. \quad \text{(A10)}$$

The limit of Eq. (A10) can then be taken as $\omega \to 0$ in order to find the maximum capacitance (C_{max} in Eq. (4))

$$\lim_{\omega\to 0} C_{pn} = C_j + C_t, \quad \text{(A11)}$$

$$\lim_{\omega\to 0} G_{pn} = \frac{1}{R_j}, \quad \text{(A12)}$$

$$\lim_{\omega\to 0} B_{pn} = 0, \quad \text{(A13)}$$

thus

$$C_{\max} = \lim_{\omega\to 0} C_{total} = \frac{\tau_{SB} R_{SB} + (C_j + C_t) R_j^2}{(R_{SB} + R_j)^2}. \quad \text{(A14)}$$

APPENDIX B: ECM FIT PARAMETERS FOR ZnO/Cu_2O

Tables III and IV present the circuit model parameters and standard deviation for fits of the admittance data for a ZnO/Cu_2O device.

TABLE III. Resulting circuit model fit parameters (using the model in Figure 4(c)) of data for a ZnO/Cu_2O device for different measurement temperatures. Fit parameters were obtained using the LEVMW nonlinear linear least squares regression fitting software.[17] The resulting differential capacitance using these parameters is laid over the data in Figure 5(a). Q and n are components of the CPE from Eq. (15). The device area was 0.15 cm^2.

T/K	R_t/Ω	Q_t	n_t	R_j/Ω	C_j/F
292	2.7×10^3	8.2×10^{-8}	0.83	1.8×10^4	5.9×10^{-10}
300	1.6×10^3	7.4×10^{-8}	0.84	1.5×10^4	6.1×10^{-10}
305	1.1×10^3	7.6×10^{-8}	0.85	1.0×10^4	6.2×10^{-10}
310	7.3×10^2	7.6×10^{-8}	0.86	8.1×10^3	6.3×10^{-10}
314	5.3×10^2	7.7×10^{-8}	0.86	6.9×10^3	6.5×10^{-10}
318	3.8×10^2	7.8×10^{-8}	0.86	5.6×10^3	6.9×10^{-10}
T/K	R_{SB}/Ω	Q_{SB}	n_{SB}	R_s/Ω	L/H
292	7.8×10^3	2.0×10^{-9}	0.92	1.6×10^{-8}	1.0×10^{-6}
300	4.4×10^3	2.9×10^{-9}	0.90	1.6×10^{-8}	1.0×10^{-6}
305	2.8×10^3	3.7×10^{-9}	0.89	1.6×10^{-8}	9.9×10^{-7}
310	1.9×10^3	5.6×10^{-9}	0.87	1.6×10^{-8}	9.8×10^{-7}
314	1.5×10^3	8.0×10^{-9}	0.85	1.6×10^{-8}	9.7×10^{-7}
318	1.3×10^3	9.9×10^{-9}	0.84	1.6×10^{-8}	9.6×10^{-7}

TABLE IV. Standard deviation of the circuit model fit parameters (Table III) reported by the LEVMW fitting software. Q and n are components of the CPE from Eq. (15). The device area was 0.15 cm^2.

T/K	R_t/Ω	Q_t	n_t	R_j/Ω	C_j/F
292	45.3	1.2×10^{-9}	2.1×10^{-3}	40.4	4.6×10^{-12}
300	21.8	7.3×10^{-10}	1.3×10^{-3}	20.4	4.0×10^{-12}
305	13.8	6.0×10^{-10}	9.6×10^{-4}	11.9	4.0×10^{-12}
310	9.9	6.0×10^{-10}	9.5×10^{-4}	9.24	4.4×10^{-12}
314	7.3	6.6×10^{-10}	1.0×10^{-3}	8.18	4.7×10^{-12}
318	4.9	6.7×10^{-10}	1.0×10^{-3}	6.63	5.2×10^{-12}
T/K	R_{SB}/Ω	Q_{SB}	n_{SB}	R_s/Ω	L/H
292	32.6	1.6×10^{-9}	6.8×10^{-4}	9.3×10^{-3}	1.3×10^{-8}
300	15.7	1.8×10^{-9}	7.4×10^{-4}	9.3×10^{-3}	1.5×10^{-8}
305	9.5	1.8×10^{-9}	8.3×10^{-4}	9.3×10^{-3}	2.1×10^{-8}
310	6.8	2.2×10^{-9}	1.6×10^{-3}	9.3×10^{-3}	2.2×10^{-8}
314	5.3	2.9×10^{-9}	1.4×10^{-3}	9.3×10^{-3}	2.0×10^{-8}
318	4.1	3.2×10^{-9}	1.5×10^{-3}	9.3×10^{-3}	1.8×10^{-8}

[1] K. P. Musselman, A. Marin, A. Wisnet, C. Scheu, J. L. MacManus-Driscoll, and L. Schmidt-Mende, Adv. Funct. Mater. **21**, 573 (2011).
[2] R. Scheer, J. Appl. Phys. **105**, 104505 (2009).
[3] H. Wilhelm, H. W. Schock, and R. Scheer, J. Appl. Phys. **109**, 084514 (2011).
[4] R. Herberholz, M. Igalson, and H. W. Schock, J. Appl. Phys. **83**, 318 (1998).
[5] A. Darga, Z. Djebbour, D. Mencaraglia, A. Migan Dubois, J. P. Connolly, J. F. Guillemoles, and D. Lincot, Phys. Status Solidi C **5**, 3449 (2008).
[6] W. A. Strifler and C. W. Bates, J. Appl. Phys. **71**, 4358 (1992).
[7] T. Walter, R. Herberholz, C. Müller, and H. W. Schock, J. Appl. Phys. **80**, 4411 (1996).
[8] M. Burgelman and P. Nollet, Solid State Ionics **176**, 2171 (2005).
[9] W. A. Hill and C. C. Coleman, Solid-State Electron. **23**, 987 (1980).
[10] J. V. Li, X. Li, Y. Yan, C. S. Jiang, W. K. Metzger, I. L. Repins, M. A. Contreras, and D. H. Levi, J. Vac. Sci. Technol. B **27**, 2384 (2009).
[11] T. Eisenbarth, T. Unold, R. Caballero, C. A. Kaufmann, and H. W. Schock, J. Appl. Phys. **107**, 034509 (2010).
[12] J. V. Li, S. W. Johnston, X. Li, D. S. Albin, T. A. Gessert, and D. H. Levi, J. Appl. Phys. **108**, 064501 (2010).
[13] S. Rühle and D. Cahen, J. Phys. Chem. B **108**, 17946 (2004).
[14] D. C. Iza, D. Muñoz-Rojas, Q. Jia, B. Swartzentruber, and J. L. MacManus-Driscoll, Nanoscale Res. Lett. **7**, 655 (2012).
[15] K. L. Chopra, P. D. Paulson, and V. Dutta, Prog. Photovoltaics **12**, 69 (2004).
[16] J. Tang and E. H. Sargent, Adv. Mater. **23**, 12 (2011).
[17] J. R. M. E. Barsoukov and J. R. Macdonald, *Impedance Spectroscopy: Theory, Experiment, and Applications*, 2nd ed. (Wiley & Sons, Inc., Hoboken, NJ, 2005), p. 34.
[18] Y. Y. Proskuryakov, K. Durose, B. M. Taele, and S. Oelting, J. Appl. Phys. **102**, 024504 (2007).
[19] J. Katayama, K. Ito, M. Matsuoka, and J. Tamaki, J. Appl. Electrochem. **34**, 687 (2004).
[20] M. Izaki, T. Shinagawa, K. T. Mizuno, Y. Ida, M. Inaba, and A. Tasaka, J. Phys. D: Appl. Phys. **40**, 3326 (2007).
[21] K. P. Musselman, A. Marin, L. Schmidt-Mende, and J. L. MacManus-Driscoll, Adv. Funct. Mater. **22**, 2202 (2012).
[22] T. Minami, Y. Nishi, T. Miyata, and J. Nomoto, Appl. Phys. Express **4**, 062301 (2011).
[23] K. P. Musselman, T. Gershon, L. Schmidt-Mende, and J. L. MacManus-Driscoll, Electrochim. Acta **56**, 3758 (2011).
[24] S. Jeong, S. H. Song, K. Nagaich, S. A. Campbell, and E. S. Aydil, Thin Solid Films **519**, 6613 (2011).
[25] A. Mittiga, E. Salza, F. Sarto, M. Tucci, and R. Vasanthi, Appl. Phys. Lett. **88**, 163502 (2006).
[26] Y. Nishi, T. Miyata, and T. Minami, J. Vac. Sci. Technol. A **30**, 04D103 (2012).
[27] W. G. Oldham and A. G. Milnes, Solid-State Electron. **7**, 153 (1964).
[28] M. Izaki and T. Omi, Appl. Phys. Lett. **68**, 2439 (1996).
[29] J. T. Heath, J. D. Cohen, and W. N. Shafarman, J. Appl. Phys. **95**, 1000 (2004).
[30] J. Kneisel, K. Siemer, I. Luck, and D. Bräunig, J. Appl. Phys. **88**, 5474 (2000).
[31] A. Niemegeers and M. Burgelman, J. Appl. Phys. **81**, 2881 (1997).
[32] See supplementary material at http://dx.doi.org/10.1063/1.4799633 for apparent trap state percent error.
[33] S. M. Sze, *Physics of Semiconductor Devices*, 3rd ed. (John Wiley & Sons, New York, 1981), p. 79.
[34] P. A. Fernandes, A. F. Sartori, P. M. P. Salomé, J. Malaquias, A. F. da Cunha, M. P. F. Graça, and J. C. González, Appl. Phys. Lett. **100**, 233504 (2012).
[35] M. Burgelman, P. Nollet, and S. Degrave, Thin Solid Films **361–362**, 527 (2000).
[36] B. N. Illy, A. C. Cruickshank, S. Schumann, R. D. Campo, T. S. Jones, S. Heutz, M. A. McLachlan, D. W. McComb, D. J. Riley, and M. P. Ryan, J. Mater. Chem. **21**, 12949 (2011).
[37] J. H. Werner and H. H. Güttler, J. Appl. Phys. **69**, 1522 (1991).
[38] U. Rau and J. H. Werner, Appl. Phys. Lett. **84**, 3735 (2004).
[39] J. Han, P. Q. Mantas, and A. M. R. Senos, J. Eur. Ceram. Soc. **22**, 49 (2002).
[40] B. Hoex, S. B. S. Heil, E. Langereis, M. C. M. van de Sanden, and W. M. M. Kessels, Appl. Phys. Lett. **89**, 042112 (2006).
[41] A. S. Gudovskikh, J.-P. Kleider, J. Damon-Lacoste, P. Roca i Cabarrocas, Y. Veschetti, J.-C. Muller, P.-J. Ribeyron, and E. Rolland, Thin Solid Films **511–512**, 385 (2006).
[42] J. Yuan, H. Shen, H. Huang, and X. Deng, J. Appl. Phys. **110**, 104508 (2011).

[43]L. Schmidt-Mende and J. L. MacManus-Driscoll, Materials Today **10**, 40 (2007).
[44]G. K. Paul, Y. Nawa, H. Sato, T. Sakurai, and K. Akimoto, Appl. Phys. Lett. **88**, 141901 (2006).
[45]A. Mittiga, F. Biccari, and C. Malerba, Thin Solid Films **517**, 2469 (2009).
[46]K. Mizuno, M. Izaki, K. Murase, T. Shinagawa, M. Chigane, M. Inaba, A. Tasaka, and Y. Awakura, J. Electrochem. Soc. **152**, C179 (2005).